

# Determination of the solar calibration constant for a sun-sky radiometer: proposal of an *in-situ* procedure

Monica Campanelli, Teruyuki Nakajima, and Bruno Olivieri

A new procedure is presented for determining *in situ* the solar calibration constant, i.e., the Sun-sky radiometer counts for a direct normal solar flux extrapolated to the top of the atmosphere. The method makes use of a modified version of the Langley plot based on the use of an inversion code of column-integrated aerosol size distribution, and it is ordinarily applied to calibrate Prede Sun-sky radiometers. To analyze how such an *in situ* method can work accurately, the technique has been applied to a five-month dataset obtained from measurements taken in Rome, Italy, by a Prede Sun-sky radiometer from 22 April to 5 November 2001. The precision of the *in situ* method has been estimated to within 1–2.5%, depending on the wavelength. © 2004 Optical Society of America

OCIS codes: 010.1290; 010.1110.

## 1. Introduction

The determination of the calibration constant  $F_0$ , i.e., the Sun-sky radiometer counts for a direct normal solar flux extrapolated to the top of the atmosphere<sup>1</sup> and is an important issue for the estimation of the aerosol optical thickness from ground-based Sun-sky radiometer measurements. Because as an error of 10% in the estimation of  $F_0$  takes an uncertainty in the retrieval of the aerosol optical thickness of about 0.1, a good accuracy is needed in its determination.

Different calibration schemes are used to obtain calibration constants of Sun-sky radiometers in the two Sun-sky radiometer networks, i.e., the Aeronet Cimel Sun-skyphotometers and the Skynet Prede skyradiometers. For the first type each instrument is checked every 6 months at the NASA Goddard Space Flight Center, Maryland, by means of an intercalibration with reference instruments located. The Aeronet reference instruments, in their turn, are typically calibrated at Mauna Loa site, Hawaii, every

2–3 months by use of the normal Langley plot technique, and  $F_0$  is determined with an accuracy of approximately 0.2–0.5%.<sup>2</sup> Intercalibration of the other Sun-sky photometers against the reference instruments is performed before deployment in the field as well as after removal, with an accuracy of 1–2%. A linear rate of change in time of  $F_0$  is then assumed in the processing of the data from field sites. The uncertainty in aerosol optical thickness due to the calibration uncertainty for the field instruments has been estimated to be approximately 0.01 to 0.02.

The Skynet Prede skyradiometer is, on the contrary, directly calibrated *in situ* by means of an improved version of the Langley plot (called the Improved Langley plot), based on the use of an inversion code for aerosol size distribution called the Skyrad code,<sup>3</sup> avoiding the problems connected to the shipping of the instruments for the calibration. In addition, because the calibration is made daily, a variation of  $F_0$  due to instrumental drift can be quickly spotted, and then appropriate corrections to data can be applied exactly from the period in which the deviation occurred. But there is not enough investigation into how such an *in-situ* method can work accurately compared with the Aeronet method, other than report by Tanaka *et al.*<sup>4</sup>

The purpose of this paper is to present a procedure for determining  $F_0$  directly *in situ*, using the Improved Langley plot technique and to show the results of its application to a 5-month dataset.

M. Campanelli (m.campanelli@isac.cnr.it) and B. Olivieri are with the Consiglio Nazionale delle Ricerche, Istituto di Scienze dell' Atmosfera e del Clima, Research Area at Roma Tor Vergata, Via del Fosso del Vavaliere 100, 00133 Rome, Italy. T. Nakajima is with the Centre for Climate System Research, University of Tokyo 4-6-1 Komaba, Meguro-ku, Tokyo 154-8904, Japan.

Received 7 May 2003; revised manuscript received 14 October 2003; accepted 17 October 2003.

0003-6935/04/030651-09\$15.00/0

© 2004 Optical Society of America

## 2. Improved Langley Plot Method

Let us consider the expression of Beer's law, implying the dependence on  $\lambda$ :

$$\ln F = \ln F_0 - \frac{\tau}{\mu_0}, \quad (1)$$

where  $F$  is the direct solar irradiance,  $\tau$  is the extinction optical thickness, and  $\mu_0 = \cos \theta_0$  is the cosine of the solar zenith angle  $\theta_0$ , if the sun is not too close to the horizon. The normal Langley plot technique consists in retrieving  $F_0$  from the plot of  $\ln F$  vs  $1/\mu_0$ , assuming that, in the selected time period, the optical thickness  $\tau$  is constant, so data must be accurately chosen because the result is directly related to the variability of  $\tau$ . Shaw<sup>5</sup> demonstrated that the linear dependence of  $\tau$  on  $\mu_0$ , which means a temporal change of the optical thickness because  $\mu_0$  depends on time, corresponds to the second-order variation in terms of time. Limiting to the first order we have

$$\tau(\mu_0) = \tau(0) + \left. \frac{\partial \tau}{\partial \mu_0} \right|_0 (\mu_0 - 0) = \tau_0 + \tau_1 \mu_0. \quad (2)$$

If we put Eq. (2) into Eq. (1) we obtain

$$\ln F = \ln F_0 - \tau_1 - \frac{\tau_0}{\mu_0}. \quad (3)$$

The variability of  $\tau$  and  $\tau_1$  in the normal Langley plot is contained in the intercept value  $\ln F_0 - \tau_1$  obtained from the fit of  $\ln F$  versus  $1/\mu_0$ , and the retrieved  $F_0$  value has a substantial dependence on the daily variability of  $\tau$ . On the other hand the Improved Langley plot retrieves  $F_0$  by the fit of  $\ln F$  versus  $\tau/\mu_0$ , including the variability  $\tau_1$  in  $\tau$ . In contrast to the normal method, the intercept  $F_0$  does not depend on the daily variability of  $\tau$ , if the column aerosol size distribution is correctly retrieved by the inversion process. In fact, to estimate the diurnal behavior of the aerosol optical thickness, we estimate the aerosol column size distribution using the Skyrad code.<sup>3</sup> This code consists of an efficient multiple scattering radiative transfer scheme<sup>6</sup> and an inversion scheme that is able to retrieve the columnar aerosol volume distribution  $v(r)$ , the extinction aerosol optical thickness  $\tau^{\text{ext}}(\lambda)$  at several wavelengths  $\lambda$ , the phase function  $P(\lambda, \Theta)$  for several scattering angles  $\Theta$ , and the single-scattering albedo  $\omega(\lambda)$ , from measured direct  $F$  (in watt meter<sup>-2</sup> micrometer<sup>-1</sup>) and diffuse  $E$  (in watt meter<sup>-2</sup> micrometer<sup>-1</sup>) solar irradiance in the Almucantar and Principal Plane geometries.<sup>7</sup>

To understand the main idea on which this method is based, we define two observable quantities by Sun-sky radiometer:

$$\ln F(\lambda) = \ln F_0(\lambda) - m_0 \tau_{\text{dir}}^{\text{ext}}(\lambda) - m_0 (\tau_{O_3} + \tau_m), \quad (4)$$

$$R(\lambda, \Theta) = \frac{L(\lambda, \Theta)}{F(\lambda) m_0} = \frac{E(\lambda, \Theta)}{\Delta \Omega(\lambda) F(\lambda) m_0}, \quad (5)$$

where  $m_0 = 1/\cos \theta_0$  is the optical air mass;  $\tau_{O_3}$  and  $\tau_m$  are the extinction optical thickness of ozone and molecules, respectively;  $\tau_{\text{dir}}^{\text{ext}}(\lambda)$  is the extinction aerosol optical thickness obtained from direct solar irradiance measurements, after the determination of  $F_0(\lambda)$ ;  $L(\lambda, \Theta)$  is the solar diffuse radiance; and  $\Delta \Omega(\lambda)$  is the solid-view angle of the instrument optics. The Aeronet uses a lamp calibration to determine the solid-view angle or transfer constant from the instrument output of measured sky irradiance  $E$  to the radiance  $L$  using an integrating sphere at the NASA Goddard Space Flight Center. Conversely, the Sky-net retrieves *in situ* the solid-view angle using a solar disk scanning technique.<sup>8</sup>

The normalized radiance  $R(\lambda, \Theta)$  can be determined as the solution of the radiative-transfer equation, as expressed as follows in the Almucantar geometry for a one-layer plane-parallel atmosphere:

$$R(\lambda, \Theta) = \omega(\lambda) \tau(\lambda) P(\lambda, \Theta) + q(\Theta) \\ = \beta(\lambda, \Theta) + q(\lambda, \Theta), \quad (6)$$

where  $q(\lambda, \Theta)$  indicates the multiple-scattering contribution and  $\beta(\lambda, \Theta)$  is the differential scattering coefficient that is equal to the single-scattering contribution. Two modalities of inversion for aerosol properties are allowed: by use of only  $R$  data, and by use of both  $R$  and  $F$  data after a previous determination of  $F_0$ . In both cases, the differential scattering coefficient  $\beta(\lambda, \Theta)$  is obtained from measured values of  $R$  by an iterative regression incorporating a multiple-scattering algorithm. Then the size distribution  $v(r)$  is finally derived from  $\beta$  and  $\tau$  data by the inversion scheme, and their expression is given by the Mie theory. The retrieved  $v(r)$  is further used to reconstruct  $\tau$  and  $\beta(\lambda, \Theta)$ , hence  $F$  and  $R$ , to compare with the measured values. The iteration stops when the rms relative deviation,  $\varepsilon(R)$  or  $\varepsilon(F, R)$ , between the measured and the calculated quantities averaged over the measured scattering angles and wavelengths, becomes less than a convergence criterion.

To apply this procedure and obtain successful results, we need appropriate values of the complex refractive index,  $m-ik$ , and ground albedo  $A$  as input parameters. It has been illustrated by numerical simulations in Nakajima *et al.*<sup>3</sup> that the normalized radiance  $R$  (and hence the phase function, being in the single-scattering approximation  $R \approx \omega \tau P$ ) has a dependence on  $m$  in the angular interval  $3^\circ \leq \Theta \leq 30^\circ$ , while at the same time in this interval there is an insignificant dependence on  $k$  and  $A$ . Moreover, the variation of  $R$  with  $k$  is almost constant from  $30^\circ$  to  $160^\circ$ , whereas from  $90^\circ$  to  $120^\circ$  there is a large variation of  $R$  on  $A$ . It leads to the conclusion that through measurement of nearly forward scattered sunlight, the result depends mainly on the real component of the refractive index, whereas measuring the scattered light at almost sideways angles of scattering the results are quite highly dependent on the refractive index and the surface albedo.

This is essentially the main idea that led to the setup of the two procedures, described in the follow-

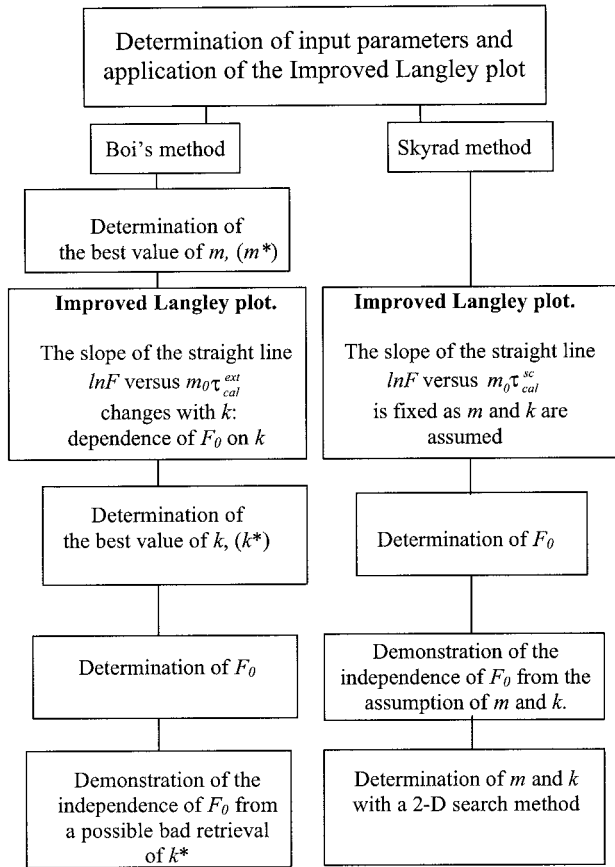


Fig. 1. Schematic diagram resuming two applications of the Improved Langley plot.

ing subsections, for the determination of the input parameters  $m$ ,  $k$ ,  $A$ , and  $F_0$  from the irradiance measurements themselves; one is proposed by Boi *et al.*<sup>8</sup> (called Boi's method), and the other is used in the version 3 of the Skyrad code (called the Skyrad method).

#### A. Skyrad Method

This method proposes to retrieve the solar calibration constant using the Improved Langley plot and then to invert data to obtain the aerosol optical and physical characteristics included the complex refractive index. With more details, the procedure, as summarized in Fig. 1, can be divided into two steps:

1) *Determination of  $F_0(\lambda)$* : Data of  $R(\Theta, \lambda)$  within the forward-scattering range  $3^\circ \leq \Theta \leq 30^\circ$  with a preassigned value of  $m$ ,  $k$ , and  $A$  are inverted. The Improved Langley plot is then applied for determining  $F_0(\lambda)$ . Considering that  $\tau^{\text{ext}}(\lambda) = [\tau^{\text{sc}}(\lambda)]/[\omega(\lambda)]$ , Eq. (4) can be written as

$$\ln F(\lambda) + m_0(\tau_{O_3} + \tau_m) = \ln F_0(\lambda) - c' m_0 \tau_{\text{cal}}^{\text{sc}}(\lambda), \quad (7)$$

where  $c' = 1/\omega(\lambda)$ , and  $\tau_{\text{cal}}^{\text{sc}}(\lambda)$  is the aerosol scattering optical thickness calculated by the inversion process of the forward-scattering sky radiance data. The retrieved optical thickness can include an error

caused by the inversion process and also by an improper preassigning of the refractive index, so that the slope of the straight line, i.e., the coefficient  $c$ , can change. But primarily it is expected this coefficient tends to be constant when the aerosol refractive index does not change significantly during the observation period for the Langley plot; in addition Eq. (6) ensures that the aerosol optical thickness for scattering is retrieved more accurately than the optical thickness for extinction. Consequently Eq. (7) is used to determine the intercept  $F_0$  by fitting  $\ln F(\lambda) + m_0(\tau_{O_3} + \tau_m)$  versus  $m_0 \tau_{\text{cal}}^{\text{sc}}(\lambda)$ .

2) *Determination of  $m$  and  $k$* : Both direct and diffuse data in the angular range  $3^\circ \leq \Theta \leq 160^\circ$  are used to retrieve  $v(r)$ ,  $m$ , and  $k$  simultaneously by means of a two-dimensional nonlinear search method that selects an optimum value of the refractive index ( $m^C$ ,  $k^C$ ) from a grid table made of several pairs of ( $m_i$ ,  $k_i$ ) so as to minimize  $\varepsilon(R)$  when  $v(r)$  is inverted.

#### B. Boi's Method

This method proposes to retrieve the solar calibration constant after the determination of the other input parameters. The real part of the refractive index is retrieved through inversion of data in the forward-scattering sunlight area, whereas the Improved Langley plot method is used to retrieve firstly the best value of the imaginary part and secondly the solar calibration constant. In fact, the slope of the straight line in the Improved Langley plot changes for various  $k$  used in the inversion process, as indicated by Eq. (7). Hence one can infer  $k$  by choosing one among the different slopes computed for several imaginary indices, as explained later, and the corresponding intercept is adopted as  $F_0$ . In detail the method, as summarized in Fig. 1, can be divided in four steps.

1) *Determination of  $m$* . An optimal value  $m^*$  for  $m$  can be determined from the minimum exhibited by the parameter  $\varepsilon(R)$  versus  $m$  in the  $3^\circ \leq \Theta \leq 30^\circ$  interval. To reduce the noise and to obtain the consistency with the values of  $k$  to be determined in the next step,  $\varepsilon(R)$  versus  $m$  is averaged over all sets of data to yield one or two representative values (one in the morning and one in the afternoon) of  $m^*$  per day, depending on the diurnal variation of data and on their quality. The retrieved  $m^*$  is assumed to be independent of wavelength, because the wavelength dependence of  $\varepsilon(R)$  is of the secondary order of magnitude for our purpose of obtaining the calibration constant.

2) *Determination of  $k$* . The Improved Langley plot is applied to retrieve the optimal  $k$  value ( $k^*$ ). In this case the following equation:

$$\ln F(\lambda) + m_0(\tau_{O_3} + \tau_m) = \ln F_0(\lambda) - c m_0 \tau_{\text{cal}}^{\text{ext}}(\lambda) \quad (8)$$

is used for fitting  $\ln F(\lambda) + m_0(\tau_{O_3} + \tau_m)$  versus  $m_0 \tau_{\text{cal}}^{\text{ext}}(\lambda)$ , where  $\tau_{\text{cal}}^{\text{ext}}(\lambda)$  is the aerosol extinction optical thickness retrieved with  $m^*$  and indicative values of  $k$ . The slope of the plot has a substantial dependence on  $k$ , as shown in Fig. 2. When the



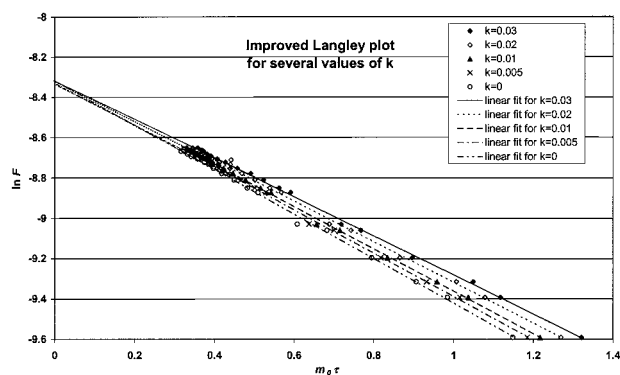


Fig. 2. Application of the Improved Langley plot for several values of  $k$ . Notice the dependence of the slope of the straight line on the imaginary part of the refractive index.

value of  $k$  is correct the  $c$  value should be 1, so that the optimal value  $k^*$  can be determined from the minimum of the parameter  $\varepsilon_C$  versus  $k$ :

$$\varepsilon_C = \left[ \frac{\sum_{\lambda} (|c(\lambda)| - 1)^2}{N_{\lambda}} \right]^{1/2}. \quad (9)$$

Two  $k^*$  values for all the wavelengths can be retrieved, one for the morning and the other for the evening, if data are available, with an expectation that the time independency of  $k^*$ , which is needed for the algorithm, tends to be established within morning and afternoon separately. Once determined  $m^*$  and  $k^*$ , the Improved Langley plot can be used to retrieve a first estimation of the intercept  $F_0(\lambda)$  by use of Eq. (4).

3) *Determination of  $A$ .* Data of  $R(\Theta, \lambda)$  in the angular range  $60^\circ \leq \Theta \leq 90^\circ$  is reconstructed by use of  $v(r)$  and  $\tau_{\text{cal}}^{\text{ext}}(500 \text{ nm})$  obtained in the second step 2 for  $m^*$ ,  $k^*$ , and several trial values of  $A$ . From the minimum of the parameter  $\varepsilon(R)$  for each  $\lambda$ , rough values of  $A$  ( $A^\circ$ ) are determined for each hour. Using  $m^*$ ,  $k^*$ , and  $A^\circ$ ,  $R(\Theta, \lambda)$  data are inverted in  $30^\circ \leq \Theta \leq 60^\circ$ , and then  $v(r)$  and  $\tau_{\text{cal}}^{\text{ext}}(500 \text{ nm})$  are updated to start a new iteration cycle. The procedure stops when for each component of  $A$  the difference between the preceding and the successive value in the cycle is less than or equal to 3%.

Finally, with use of determined  $m^*$ ,  $k^*$ , and  $A^*$  the Improved Langley plot is applied again to retrieve the  $F_0(\lambda)$  value and then  $\tau_{\text{dir}}^{\text{ext}}(\lambda)$  by use of Eq. (4). Data of  $R(\Theta, \lambda)$  together with  $\tau_{\text{dir}}^{\text{ext}}(\lambda)$ , calculated in the last point, can be now inverted to retrieve a better estimation of  $v(r)$ ,  $\tau_{\text{cal}}^{\text{ext}}(\lambda)$ ,  $P(\Theta)$ , and  $\omega(\lambda)$ .

The last step is proved not necessary to the procedure, as it does not improve the results obtained at the end of the third step. This is because the information content included in the direct measurements (i.e.,  $\tau_{\text{dir}}^{\text{ext}}$  retrieved at the last step) has just been used in the Improved Langley plot (second step) for the determination of  $k$ . In addition,  $F_0(\lambda)$  retrieved at the final step after the determination of  $A$  is shown to not be very different from that retrieved at the

second step. For this reasons, only the first two steps of the procedure will be treated in this work.

The Boi and Skyrad procedures are not very different from each other. Concerning the determination of the refractive index, the use of direct and diffuse irradiance improves the accuracy of retrieving  $k$ . In fact the direct irradiance includes the information given by the extinction optical thickness, and diffuse irradiance includes the information given by the scattering optical thickness, so that the simultaneous use of direct and diffuse irradiances lead to more accurate retrieval of  $\omega$ , and hence  $k$ . In Boi's method, the Improved Langley plot uses both the information (direct and diffuse) for the determination of  $k$ , whereas in the Skyrad method, direct and diffuse measurements are used together in the inversion.

Concerning the determination of the solar calibration constant, in both methods,  $F_0$  retrieved by the fit, is used to determine  $\tau_{\text{dir}}^{\text{ext}}$ , whereas Boi's method takes into account the dependence of the slope of the straight line on the refractive index, i.e., the atmospheric absorption information included in the temporal variation of the direct and diffuse irradiance, to retrieve a good calibration constant. The Skyrad method does not use this dependence to derive  $F_0$ . In fact, in this case from the inversion of  $R$  data within the interval  $0^\circ \leq \Theta \leq 30^\circ$  with a prescribed value of  $m$  and  $k$ ,  $\tau_{\text{cal}}^{\text{sc}}$  is retrieved relatively accurately, because it is nearly proportional to the differential cross section, which also does not have a strong dependence on  $m$  and  $k$  in the forward-scattering range. In fact, the forward lobe of the phase function is caused mainly by the Fraunhofer diffraction phenomenon, which is determined by the shape of the particle: Radiation traveling over the particle is diffracted as forward scattering. This diffraction acts in a similar way in an opaque object as well as in transparent ones. This means the forward lobe is relatively independent of the refractive index of the particle, even though there is always some dependence on the assumed values of the complex refractive index. Furthermore, in cases of turbid atmosphere, multiple scattering correction introduces a dependence on the  $k$  value. Once assumed  $m$  and  $k$ ,  $\tau_{\text{cal}}^{\text{sc}}$  and  $\omega$  can be calculated from the inversion, and the intercept  $F_0$  can be determined accurately because the coefficient  $c' = 1/\omega$  in Eq. (7) is a weak function of time. The single-scattering albedo becomes a strong function of time and hence a function of optical thickness only when the refractive index is markedly a function of time. In this case the intercept could have a dependence on  $k$  and  $m$ .

### 3. Results

The two methods have been applied to a data set of measurements taken on the roof of the building of the University Engineering Department in the center of Rome, by the sky radiometer Prede model Pom 01L. They were taken from 22 April to 4 July and from 25 October to 5 November 2001 and were selected in order to have clear-sky measurements only. The

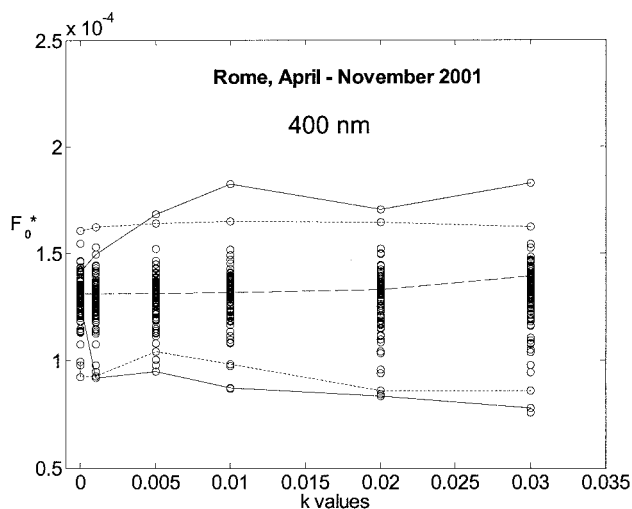


Fig. 3.  $F_0^*$  versus  $k$  at 400 nm, retrieved for all the days. The connecting line has been drawn only for five days corresponding to the following cases: the two lowest and the two highest  $F_0^*$  retrieved values (solid and dotted curves), and only one for the more frequently retrieved values (dashed curve).

Improved Langley plot was applied to data with  $m_0 > 4.5$ .

#### A. Boi's Method

We first want to show that  $F_0$  calculated with Boi's method does not depend on the variability of  $\tau_{\text{cal}}^{\text{ext}}$  owing to a wrong retrieval of  $k^*$  in both turbid and clean atmospheres. For this purpose the following two steps have been considered:

- 1)  $F_0$  determined with  $\tau_{\text{cal}}^{\text{ext}}$  retrieved for  $m^*$  and several values of  $k$ , ( $F_0^*$ ).
- 2)  $F_0$  determined with  $\tau_{\text{cal}}^{\text{ext}}$  retrieved for  $m^*$  and  $k^*$ , ( $F_0^{**}$ ).

Seven values of  $k$  were used (0.03, 0.02, 0.01,  $5 \times 10^{-3}$ ,  $1 \times 10^{-3}$ ,  $1 \times 10^{-5}$ , and 0) for the tests, and  $m^*$  was determined previously with the above-mentioned method, for each day. This value was used to determine  $\tau_{\text{cal}}^{\text{ext}}$  and then  $F_0^*$ . Figure 3 shows the behavior of  $F_0^*$  thus obtained versus  $k$  at  $\lambda = 0.400 \mu\text{m}$ . Then, the mean value over all values of  $k$ , the standard deviation, and the percentage relative error were calculated for each day. Since this error oscillates during the period, the average value and the standard deviation ( $\sigma$ ) over time of the percentage relative errors were calculated in order to estimate the mean dependence of  $F_0^*$  on  $k$ . Accord-

Table 1. Boi's Method. Mean Percentage Dependence of  $F_0^*$  on  $k$  and Its Standard Deviation after the Selection with the Chauvenet Criterion

Dependence of $F_0^*$ on $k$ (%)			
400 nm	500 nm	870 nm	1020 nm
$1.53 \pm 1.25$	$0.85 \pm 0.74$	$0.38 \pm 0.27$	$0.30 \pm 0.21$

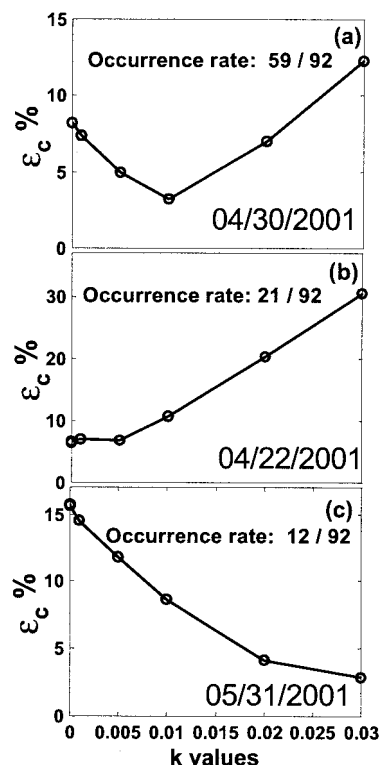


Fig. 4. Three cases of the dependence of the parameter  $\epsilon_c$  on  $k$  for the determination of  $k^*$ .

ing to the Chauvenet Criterion,<sup>9</sup> values lying out of  $3\sigma$  were rejected. As will be shown later, these outliers mostly occur on days with high turbidity of the atmosphere. As shown in Table 1, the maximum dependence is  $\sim 2.8\%$  for 400 nm and decreases with the increase of  $\lambda$  down to 0.5%. In fact, assuming that the wavelength dependence of  $\tau$  is  $\tau(\lambda) \approx \lambda^{-\alpha}$ , with  $\alpha$  being the Angstrom coefficient, for shorter  $\lambda$  (and therefore larger  $\tau$  values), the application of the Langley plot tends to become difficult, because at short wavelengths the slope of the regression line increases with increasing  $\tau$ .

Whereas the retrieval of  $F_0$  has been shown to be affected slightly by the assumption of  $k$ , the parameter  $\epsilon_c$  in Eq. (9), related to the regression coefficient of the straight line, has a strong dependence on  $k$  and shows a clear minimum at the most optimum value of  $k$ , ( $k^*$ ) [Fig. 4(a)]. Only in a few cases is the determination of  $k^*$  uncertain, as in Fig. 4(b), where a clear minimum is not recognizable, but nevertheless we guess  $k^* = 0$  is most plausible. On the other hand we have a case as in Fig. 4(c) that  $\epsilon_c$  has a decreasing behavior, suggesting  $k^* > 0.03$ .

By use of  $m^*$  and  $k^*$ ,  $F_0^{**}$  was retrieved for each day. We investigated in Fig. 5 the behavior of  $F_0^{**}$  for  $\lambda = 500 \text{ nm}$  versus time, plotted daily and superimposed on the values of  $F_0$  retrieved at the seven values of  $k$  used in the previous tests for Fig. 3. To see if there is any relationship between the retrieved  $F_0^{**}$  and the turbidity of the atmosphere, the data set was divided into three classes: (a) days with  $\tau(500$

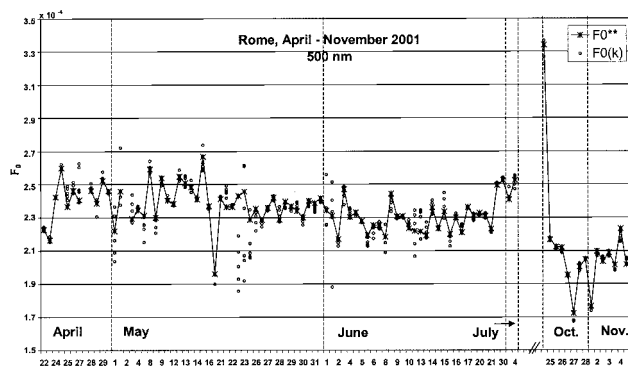


Fig. 5. Boi's method. Temporal behavior of  $F_0^{**}$  and  $F_0^*$  for several  $k$  values, at 500 nm. Two values for each day are plotted: one for the morning, the other for the evening. To put the temporal behavior in evidence, the time scale is irregularly spaced.

nm)  $< 0.1$ , (b) days with  $0.1 \leq \tau(500 \text{ nm}) < 0.3$ , and (c) days with  $\tau(500 \text{ nm}) \geq 0.3$ .

No clear dependence on  $\tau(500 \text{ nm})$  is recognizable for all the wavelengths, but it is interesting to find that small and large  $\tau$  cases seem to cause larger variability in the temporal behavior of  $F_0^{**}$ , whereas cases with medium values of  $\tau$  seem to bring relatively converging values. The reason might be that the estimation of  $k$  becomes difficult for small  $\tau$  cases, so that an error in  $k^*$  value makes the retrieval of  $F_0^{**}$  incorrect. For large  $\tau$  cases, as pointed out above, the application of the Langley plot tends to become difficult as well as the determination of  $k^*$  and  $F_0^{**}$ .

To check this hypothesis, the percentage dependence of  $F_0^*$  on  $k$  is analyzed for the three cases in Table 2. For  $\tau \geq 0.3$ ,  $F_0^*$  changes substantially with  $k$ , indicating difficulty in good determination of  $k^*$  that leads to the large variability in the retrieved  $F_0^{**}$  values. On the contrary, for  $\tau < 0.1$  the dependence of  $F_0^*$  on  $k$  is weak, apparently denying the above hypothesis. But when  $\tau$  is small, even with a large mistake in the estimation of  $k^*$ , the error in the intercept  $F_0^*$  should not be large owing to small  $\tau$ . At the same time Table 1 shows that there is a weak sensitivity of  $F_0^*$  on the assumed  $k$  values. The combination of the two reasons makes the dependence of  $F_0^*$  on  $k$  for small  $\tau$  cases not detectable.

Figure 5 indicates that the variability of  $F_0^{**}$  during the period is quite high, in spite of the small uncertainty proposed by the Improved Langley method. These errors can be caused by many reasons, such as improper cloud screening, large horizontal inhomogeneity in the aerosol stratification, mechanical noises,

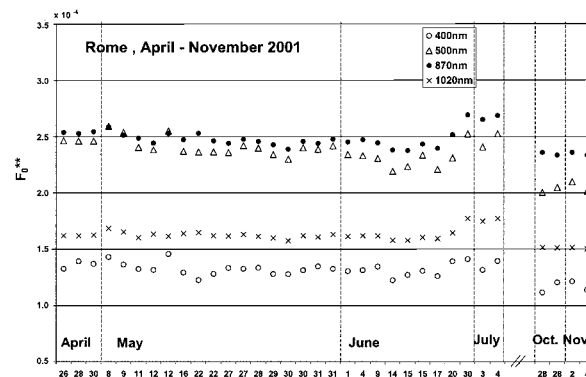


Fig. 6. Boi's method. Temporal behavior of  $F_0^{**}$  retrieved for all the wavelengths, after the quality control selection. To put the temporal behavior in evidence, the time scale is irregularly spaced.

and so on. Therefore a quality check is needed to reject improper values. In this study all the values of  $F_0^{**}$  corresponding to  $\epsilon_C \geq 5\%$  and  $\epsilon(R) \geq 5\%$  were rejected. The result plotted in Fig. 6 for each  $\lambda$  shows that the quality control successfully filters the unrealistic short-term variation from the time series. At the end of June and in July,  $F_0^{**}$  was always higher than the other ones for all four wavelengths. One reason could be related to the fact that in those days, at noon the temperature was very high (more than  $35^\circ\text{C}$ ), and the thermostat in the optical mechanism could not keep the instrument temperature constant all day long, thereby altering the measurements. In fact, the thermostat was set to keep the temperature at  $35^\circ\text{C}$ , and measurements taken at higher values cannot be considered to be reliable. Consequently, data at the end of July and June, being clearly out of the general pattern, were rejected in this study.

On the contrary, lower values are recognizable in October and November for each  $\lambda$ , and this could be a sign of deteriorating instrument performance. In fact, data taken later (December 2001) in Antarctica with the same instrument reaffirmed the decrease of  $F_0^{**}$  values.

To demonstrate the performance of this present calibration method compared with the normal Langley plot method, Fig. 7 shows the temporal behavior of  $F_0^{**}$  and  $F_0$  retrieved with the normal technique ( $F_0$  normal) at 500 nm before the quality control selection. The latter is much more variable in time as it is more dependent on the atmospheric conditions.

## B. Skyrad Method

To show the independence of  $F_0$  from the assumption of  $m$ , the Improved Langley plot was applied assum-

Table 2. Boi's Method. Mean Percentage Dependence of  $F_0^*$  on  $k$  and Its Standard Deviation for Three Cases of  $\tau$  at 500 nm

$\lambda$	Dependence of $F_0^*$ on $k$ (%)			
	400 nm	500 nm	870 nm	1020 nm
$\tau < 0.1$	$1.01 \pm 0.53$	$0.61 \pm 0.37$	$0.35 \pm 0.21$	$0.35 \pm 0.19$
$\tau \geq 0.3$	$4.58 \pm 4.32$	$2.39 \pm 2.44$	$0.93 \pm 0.71$	$0.81 \pm 0.56$
$0.1 \leq \tau < 0.3$	$1.32 \pm 1.00$	$0.76 \pm 0.58$	$0.33 \pm 0.23$	$0.27 \pm 0.23$

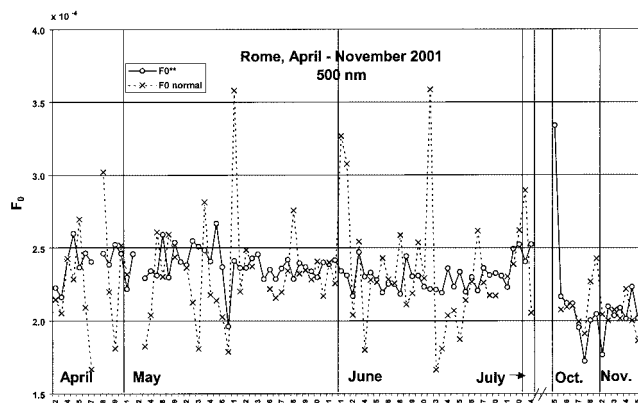


Fig. 7. Boi's method. Temporal behavior of  $F_0^{**}$  and  $F_0$  obtained from the normal Langley plot, at 500 nm, before the quality control selection. For each day two values are plotted: one for the morning and one for the evening. To put the temporal behavior in evidence, the time scale is irregularly spaced.

ing  $k = 5 \times 10^{-3}$  and several values of  $m$  (1.35, 1.40, 1.45, 1.50, 1.55, 1.60, and 1.65) to invert  $R$  data. For each day the standard deviation among the  $F_0$  values was retrieved for all  $m$ , and then the percentage relative error was calculated. The result is shown in the first row of Table 3. The Chauvenet Criterion was also applied in this analysis and after the selection the maximum dependence on  $m$  is found to be 2% at 400 nm down to 1% at 1020 nm. The selected outliers seem to be related to the days in which the temporal behavior of  $F_0$  oscillates largely. The same analysis was made for the dependence of  $F_0$  on  $k$ , using a fixed value of  $m$  (1.50) and several values of  $k$  (0.03, 0.02, 0.01, 0.005, 0.002, and 0). The results are shown in Table 3. After the selection with the Chauvenet Criterion, the maximum variability on  $k$  is demonstrated to be less than 2% at 400 nm down to 0.5% at 1020 nm. Also in this case a larger dependence on  $k$  seems to be related to the days in which the temporal behavior of  $F_0$  oscillates significantly. On the contrary,  $\omega$  retrieved from the slope of the straight line, Eq. (7), is found to be more affected by an arbitrary choice of  $k$  (Table 3). In any case this does not influence the accuracy of the retrieval of  $F_0$ .

Table 3. Mean Percentage Dependence of  $F_0$  on  $m$ ,  $k$ , and  $\omega$  and Its Standard Deviation after the Chauvenet Criterion

Skyrad Method	400 nm	500 nm	870 nm	1020 nm
Dependence of $F_0$ on $m$ (%)	$1.29 \pm 0.90$	$0.80 \pm 0.79$	$0.61 \pm 0.83$	$0.57 \pm 0.78$
Dependence of $F_0$ on $k$ (%)	$0.85 \pm 0.98$	$0.35 \pm 0.38$	$0.29 \pm 0.45$	$0.25 \pm 0.26$
Dependence of $\omega$ on $k$ (%)	$2.26 \pm 1.54$	$1.24 \pm 1.00$	$1.73 \pm 1.71$	$2.37 \pm 1.95$

Table 4. Skyrad Method. Mean Percentage Dependence of  $F_0$  on  $k$  and Its Standard Deviation for 3 Cases of  $\tau$  at 500 nm

Dependence of $F_0$ on $k$ (%)				
$\lambda$	400 nm	500 nm	870 nm	1020 nm
$\tau < 0.1$	$0.48 \pm 0.44$	$0.37 \pm 0.36$	$0.24 \pm 0.24$	$0.27 \pm 0.27$
$\tau \geq 0.3$	$2.54 \pm 2.99$	$1.6 \pm 1.16$	$0.7 \pm 1.12$	$0.48 \pm 0.59$
$0.1 \leq \tau < 0.3$	$0.48 \pm 0.44$	$0.37 \pm 0.36$	$0.24 \pm 0.24$	$0.27 \pm 0.27$

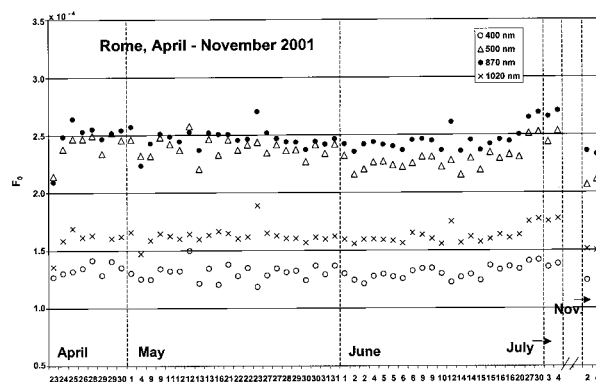


Fig. 8. Skyrad method. Temporal behavior of  $F_0$  retrieved for all the wavelengths, after the quality control selection. To put the temporal behavior in evidence, the time scale is irregularly spaced.

To identify any relationship between the retrieved  $F_0$  and the turbidity of the atmosphere, the same three cases of  $\tau(500 \text{ nm})$  used in Boi's method were analyzed, but we did not find a clear dependence of  $F_0$  on  $\tau$ . In Table 4 the percentage dependence of  $F_0$  on  $k$  is shown for the three cases of turbidity. Also in this method for  $\tau(500) > 0.3$ ,  $F_0$  is greatly dependent on  $k$ , but comparing Table 2 with Table 4 for each  $\lambda$ ,  $F_0$  retrieved with the Skyrad method is generally less dependent on  $k$  than using Boi's method in all three turbidity cases.

To retrieve  $F_0$  for our dataset,  $m = 1.50$ ,  $k = 0.01$ , and an indicative value of  $A = 0.1$  for each  $\lambda$  was assumed in the inversion. As in Boi's method, the variability of  $F_0$  from the Skyrad method during the time was quite high, and a qualified selection was needed. All values of  $F_0$  corresponding to  $\varepsilon(R) \geq 5\%$  were rejected, and the result can be seen in Fig. 8.

#### 4. Accuracy of the Calibration

The time series of the selected  $F_0$  values at 500 nm from the two methods for the analyzed period are shown in Fig. 9. The two methods do not give very different results, but in the Skyrad method the time series looks less stable. The latter method produced more number of selected points for each month but



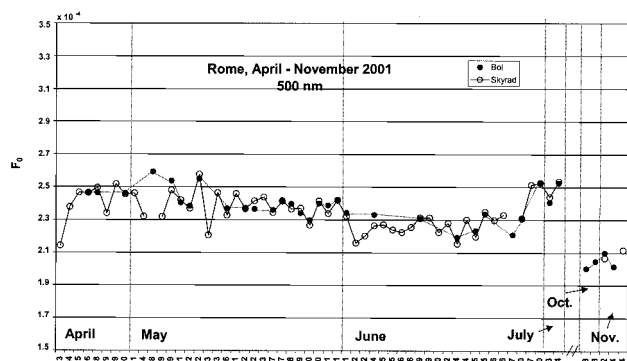


Fig. 9. Comparison between  $F_0$  retrieved by Boi's methods and the Skyrad method at 500 nm. To put the temporal behavior in evidence, the time scale is irregularly spaced.

caused the larger variability than in Boi's method (except in October, when all data was rejected), and moreover the consequence of the assumed refractive index in the Skyrad method is evident in the larger variability.

Analyzing the temporal behaviors of the series from both methods, it can be easily inferred that the

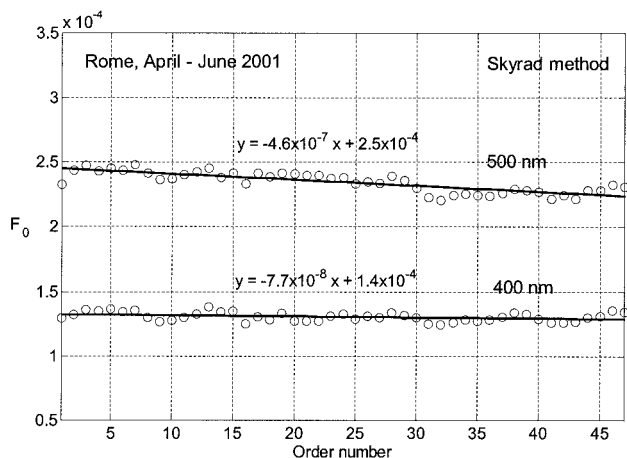
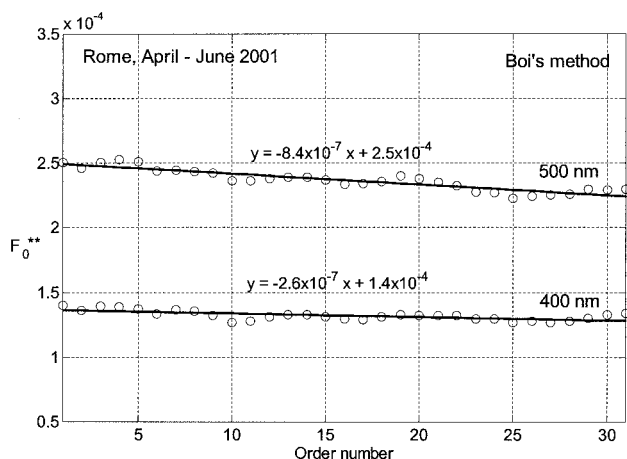


Fig. 10.  $F_0$  retrieved by the Boi's (top) and Skyrad (bottom) methods after the application of the 3-point moving average, for 500 and 400 nm; the regression line is plotted for the two series.

Table 5. Accuracy of the Retrieval of  $F_0$  with the Improved Langley Method

Accuracy of the $F_0$ Retrieval (%)				
$\lambda$	400 nm	500 nm	870 nm	1020 nm
Boi's method	2.1	1.5	1.2	0.8
Skyrad method	2.5	2.0	1.8	2.0

measure of  $F_0$  is a slowly changing function of time and the short-term variations can be related to the method itself and then to the atmospheric conditions. The long-term variations can be a sign of instrumental problems. To filter out the short-term variations, the distance of each retrieved point from the real trend of  $F_0$ , i.e., the variance of  $F_0$  series, must be minimized. To this purpose a three-point moving average was applied to both series of selected  $F_0$ . The results are shown in Fig. 10 for data from 23 April to 20 June. Data from October to November must be treated as a different series, but considering the small quantity of data recovered, the moving average can not be applied. As illustrated in Fig. 10 for Boi's method (top) and the Skyrad method (bottom), the 500-nm series after the filtering procedure shows a small decreasing trend, probably related to an instrumental drift. To estimate the accuracy of the method, as intended as internal consistency of the retrieved  $F_0$  values, the regression line of each series was estimated and the dispersion of the points with respect to the line was calculated. The resultant accuracy for both methods is reported in Table 5.

Even if Boi's method is more accurate better than the Skyrad method, as expected, both are within 2.5%, which means a good level of accuracy of the Improved Langley plot in retrieving  $F_0$  and in recognizing a trend due to instrumental degrade.

## 5. Conclusions

An *in-situ* procedure for the determination of the solar calibration constant for a Sun-sky radiometer has been presented. The method is based on the use of the Skyrad code and consists of an improved version of the Langley plot technique, where the solar calibration constant is retrieved by fitting the logarithm of the direct solar irradiance versus the product of the airmass and the extinction optical thickness, instead of only the airmass, as retrieved by the Skyrad code. Two calibration methods based on this principle were applied for a five-months data set. One is Skyrad method that retrieve the calibration constant assuming a fixed value of the refractive index to calculate the extinction optical thickness. The other is Boi's method that retrieves the calibration constant after a determination of the refractive index to be used in the retrieval of the extinction optical thickness.

The dependence on the imaginary part the refractive index was found to not exceed 2.8% for  $\lambda = 400$  nm down to 0.5% for  $\lambda = 1020$  nm in Boi's method, and 1.8% for  $\lambda = 400$  nm down to 0.5% for  $\lambda = 1020$



nm in the Skyrad method. The dependence on the real part of the refractive index was revealed to be within 2.2% for  $\lambda = 400$  nm down to 1.4% for  $\lambda = 1020$  nm in the Skyrad method. Consequently the Improved Langley technique used in both calibration methods is lightly sensitive to the variability of the optical thickness, owing to an incorrect refractive index, retrieved or assumed.

A qualified selection of the  $F_0$  data was performed, and a short-term filter was applied. As up to two values a day of  $F_0$  could be calculated, the filter was set up with the aim of retrieving the best daily calibration constant in order to quickly recognize its variation owing to instrumental drift. The accuracy of both methods was shown to be within 1–2.5%, depending on the wavelength. Although the accuracies of the Aeronet method and of the Improved Langley plot method could not be properly compared (as neither are absolute accuracies), an important result was obtained because they produced a similar uncertainty on the  $F_0$  values. This conclusion may encourage us to develop a good *in-situ* calibration method, because it avoids the problems connected with the periodical shipping of the instruments for the calibration. In addition the daily calibration allows for application of the appropriate corrections of data to be elaborated, exactly from the period in which  $F_0$  begins to decrease, instead of reanalysis of data after the calibration.

To improve the accuracy of the method, a more severe selection of the  $F_0$  data can be performed, rejecting, for example, values retrieved during days with high turbidity in the atmosphere. In fact, as shown in this paper, at  $\tau(500\text{ nm}) > 0.3 F_0$  is greatly dependent on  $k$ , both in the Skyrad and Boi's methods, and a wrong value of  $k$ , retrieved or assumed, can result in an unreliable  $F_0$ . An iteration method can be introduced to improve the Skyrad method to take

into account the information of the refractive index retrieved from all scattering-angle data. The analysis of the temporal behaviors of  $F_0$  data from measurements taken in other periods reveals that a sudden drop of the constant value can occur, for all wavelengths or only some of them, instead of a decreasing trend. In this case it is important to develop a method that can filter the series and recognize its prospective change.

## References

1. G. E. Shaw, "Error analysis of multi-wavelength sun photometry," *Pure Appl. Geophys.* **114**, 1–4 (1976).
2. B. N. Holben, T. F. Eck, I. Slutsker, D. Tanre, J. P. Buis, A. Setzer, E. Vermote, J. A. Reagan, Y. J. Kaufman, T. Nakajima, F. Lavenu, I. Jankowiak, and A. Smirnov, "AERONET—a federated instrument network and data archive for aerosol characterization," *Remote Sens. Environ.* **66**, 1–16 (1998).
3. T. Nakajima, G. Tonna, R. Rao, P. Boi, Y. Kaufman, and B. Holben, "Use of sky brightness measurements from ground for remote sensing of particulate polydispersions," *Appl. Opt.* **35**, 2672–2686 (1996).
4. M. Tanaka, T. Nakajima, and M. Shiobara, "Calibration of a sunphotometer by simultaneous measurements of direct-solar and circumsolar radiations," *Appl. Opt.* **25**, 1170–1176 (1986).
5. G. E. Shaw, "Sun photometry," *Bull. Am. Meteorol. Soc.* **64**, 4–10 (1983).
6. T. Nakajima and M. Tanaka, "Algorithms for radiative intensity calculations in moderately thick atmospheres using a truncation approximation," *J. Quant. Spectrosc. Radiat. Transfer* **40**, 51–69 (1988).
7. G. Tonna, T. Nakajima, and R. Rao, "Aerosol features retrieved from solar aureole data: a simulation study concerning a turbid atmosphere," *Appl. Opt.* **34**, 4486–4499 (1995).
8. P. Boi, G. Tonna, G. Dalu, T. Nakajima, B. Olivieri, A. Pompei, and M. Campanelli, "Procedures of calibration and data elaboration in sky radiance measurements," *Appl. Opt.* **38**, 896–907 (1999).
9. H. D. Young, *Statistical Treatment of Experimental Data* (McGraw-Hill, New York, 1962), pp. 78–80.